Available online at www.sciencedirect.com
ScienceDirect
Optics Communications 268 (2006) 146–154
OPTICS COMMUNICATIONS
www.elsevier.com/locate/optcom

All-optical switching and storage in a four-level tripod-type atomic system

M.A. Antón [a,*], Oscar G. Calderón [a], Sonia Melle [a], I. Gonzalo [b], F. Carreño [a]

[a] Escuela Universitaria de Óptica, Universidad Complutense de Madrid, C/Arcos de Jalón s/n, 28037 Madrid, Spain
[b] F. CC. Físicas, Universidad Complutense de Madrid, C/Ciudad Universitaria s/n, 28040 Madrid, Spain

Received 1 June 2006; received in revised form 27 June 2006; accepted 29 June 2006

Abstract

The optical behavior of a four-level tripod-type atomic system in a ring resonator driven by a cavity field and two external coherent fields is studied. It is shown that the atomic response exhibits an ultra-sensitive switch from high absorption to nearly transparency by changing the value of one of the control fields. The optical bistable response can be controlled by means of the external fields. The system can flip from the lower to the upper branch of the hysteresis curve without changing the incident probe. Switching and information storage of a light signal are predicted under appropriate triggering of the auxiliary external optical signals.

Keywords: Optical bistability; Optical switching; Multilevel atoms; Atomic coherence

1. Introduction

Control of light by light is essential in all-optical communication and optical computing. In the past two decades, all-optical switches based on optical bistability (OB) in two-level atomic systems have been extensively studied [1]. In traditional optical bistability systems there are limitations for applications because the only controllable optical beam is the input field, which is part of the bistable curve in the input–output plot. The situation changes when we consider multilevel atoms inside a cavity. First of all, there are new control fields between the different atomic levels, and most interestingly, new physical mechanisms such as quantum interference and coherence effects, which can greatly modify the absorption, dispersion and nonlinearity of the system. It is well known that the optical properties of atomic media may be dramatically altered if the atoms are placed into appropriate superposition of quantum states. A lot of phenomena such as electromagnetically induced transparency (EIT) [2–5], lasing without inversion (LWI) [6–9], refractive index enhancement without absorption [10,11], and spontaneous emission cancellation [12,13] have been predicted and experimentally demonstrated.

The role of atomic coherences in the context of collective phenomena, such as OB, has been subject to analysis once again. Walls et al. [14,15] and Harshawardhan and Agarwal [16] proposed a novel scheme for OB using atomic coherence effects in three-level systems. They found that in Λ-type atoms the resulting OB is due to a population trapping in a coherent superposition of the ground state sublevels. This coherent superposition is not coupled to the excited level which leads to a narrow non-absorption resonance in the absorption profile. As the intensity of the driving field increases, the non-absorption resonance dip broadens and therefore the medium becomes transparent. Recently, there has been a renewed interest in this subject from a theoretical and experimental point of view. Xiao and coworkers have shown the influence of quantum coherence effects in three-level Λ atoms such as cavity-linewidth narrowing [17], dynamic instability in an optical ring cavity [18], OB [19], and dynamical hysteresis [20] in a system formed by three-level Rubidium (Rb) atoms.

* Corresponding author. Tel.: +34 913946855; fax: +34 913946885.
E-mail address: antonm@fis.ucm.es (M.A. Antón).

0030-4018/$ - see front matter © 2006 Elsevier B.V. All rights reserved.
doi:10.1016/j.optcom.2006.06.079

Another way of generating coherence is connected with the relaxation processes such as spontaneous emission [13,21–23]. Very recently, Joshi et al. [24] studied the role of spontaneously generated coherence on OB. Similar studies have been carried out in V-type atoms [25] taking into account the possibility of quantum interference between the two decay channels from the two upper sublevels to the ground level, i.e., vacuum induced coherence. OB was achieved with considerable lower threshold intensity. OB in V-type atoms driven by a coherent field in a broadband squeezed vacuum has also been analyzed [26], showing that the width of the hysteresis loop can be controlled changing the relative phase of the squeezed vacuum to the coherent field.

Large nonlinear susceptibilities with low pumps and high sensitivities are desirable when considering the development of optical shutters, phase conjugation as well as others all-optical information processing devices. In view of these requirements it should be interesting to explore procedures and/or physical mechanics to engineer the bistable response. Chang et al. [27] and Novikova et al. [28] have reported observations of novel dynamic behavior in resonantly enhanced stimulated Raman scattering in Rb vapor. In particular, they demonstrated a dynamic hysteresis of the Raman scattered optical field. Tripod-type atoms have proved to be robust systems for engineering arbitrary coherent superposition of atomic states [29]. Paspalakis and Knight [30] have analyzed transparency, slow light and parametric generation in a medium of tripod atoms. Petrosian and Malakian [31] have shown that this system can support large magneto-optical rotation with negligible absorption. They also found a novel regime of extremely efficient nonlinear interactions of two multimode single-photon pulses. In a related work, Rebic et al. [32] have pointed out that the large Kerr cross-phase modulation among the probe and trigger fields enables one to implement a phase gate with a conditional phase shift of the order of π.

In this work we explore adequate control schema to make the advantages of multilevel atomic systems accessible for possible applications. We study the behavior of a tripod-type four-level atom in a unidirectional ring resonator driven by a cavity field and two external coherent fields. First, we analyze the linear absorption of the probe field under the influence of the control fields. It is shown that the system can switch from high absorption to nearly transparency with a large contrast ratio by varying one of the driving fields. We analyze how the hysteresis curve is modified by acting on one of the external fields without changing the incident probe field. The controlled shift of the hysteresis curve allows us the possibility of obtaining all-optical switching and storage of light signals. We illustrate the feasibility of the proposed scheme by considering experimentally accessible atomic configurations.

The paper is organized as follows: Section 2 establishes the model, i.e., the Hamiltonian of the system and the evolution equations of the atomic operators assuming the rotating wave approximation. Section 3 deals with the analysis of the linear susceptibility of the atomic system. In Section 4 we analyze the cavity field dynamics in different schema. Section 5 summarizes the main conclusions.

2. The model and the equations of motion

The scheme of levels of the atomic system we are considering is shown schematically in Fig. 1a. Here transition $|1\rangle \to |4\rangle$ is driven by a field with Rabi frequency Ω_1, while transitions $|2\rangle \to |4\rangle$ and $|3\rangle \to |4\rangle$ are driven by two control fields with Rabi frequencies Ω_2, and Ω_3, respectively. $\Delta_j = \omega_{4j} - \omega_j$ $(j = 1, 2, 3)$ denotes the detuning between the frequency of the transition $|j\rangle \to |4\rangle$ and the laser frequency ω_j. In the interaction picture and in the dipole and rotating wave approximations, the Hamiltonian of the atomic system is given by [30,32]

$$H = \hbar\Delta_1\sigma_{44} + \hbar(\Delta_3 - \Delta_1)\sigma_{33} + \hbar(\Delta_2 - \Delta_1)\sigma_{22} - \hbar(\Omega_1\sigma_{41} + \Omega_2\sigma_{42} + \Omega_3\sigma_{43} + \text{H.c.}) + \mathscr{L}\rho, \tag{1}$$

where $\mathscr{L}\rho$ stands for the dissipative Liouvillian.

The Bloch equations for the density matrix elements including atomic spontaneous emission and dephasing are

$$\begin{aligned}
\frac{\partial\rho_{44}}{\partial t} &= -(\Gamma_{41} + \Gamma_{42} + \Gamma_{43})\rho_{44} + i\Omega_1\rho_{14} - i\Omega_1^*\rho_{41} + i\Omega_2\rho_{24} - i\Omega_2^*\rho_{42} + i\Omega_3\rho_{34} - i\Omega_3^*\rho_{43},\\
\frac{\partial\rho_{33}}{\partial t} &= -(\Gamma_{32} + \Gamma_{31})\rho_{33} + \Gamma_{43}\rho_{44} + i\Omega_3^*\rho_{43} - i\Omega_3\rho_{34},\\
\frac{\partial\rho_{22}}{\partial t} &= \Gamma_{42}\rho_{44} + \Gamma_{32}\rho_{33} - \Gamma_{21}\rho_{22} + i\Omega_2^*\rho_{42} - i\Omega_2\rho_{24},\\
\frac{\partial\rho_{14}}{\partial t} &= -(\gamma_{41} - i\Delta_1)\rho_{14} + i\Omega_1^*(\rho_{44} - \rho_{11}) - i\Omega_2^*\rho_{12} - i\Omega_3^*\rho_{13},\\
\frac{\partial\rho_{13}}{\partial t} &= -[\gamma_{31} - i(\Delta_1 - \Delta_3)]\rho_{13} + i\Omega_1^*\rho_{43} - i\Omega_3\rho_{14},\\
\frac{\partial\rho_{12}}{\partial t} &= -[\gamma_{21} - i(\Delta_1 - \Delta_2)]\rho_{12} + i\Omega_1^*\rho_{42} - i\Omega_2\rho_{14},\\
\frac{\partial\rho_{23}}{\partial t} &= -[\gamma_{32} - i(\Delta_2 - \Delta_3)]\rho_{23} + i\Omega_2^*\rho_{43} - i\Omega_3\rho_{24},\\
\frac{\partial\rho_{24}}{\partial t} &= -(\gamma_{42} - i\Delta_2)\rho_{24} + i\Omega_2^*(\rho_{44} - \rho_{22}) - i\Omega_1^*\rho_{21} - i\Omega_3^*\rho_{23},\\
\frac{\partial\rho_{34}}{\partial t} &= -(\gamma_{43} - i\Delta_3)\rho_{34} + i\Omega_3^*(\rho_{44} - \rho_{33}) - i\Omega_1^*\rho_{31} - i\Omega_2^*\rho_{32},
\end{aligned} \tag{2}$$

where Γ_{ij} is the spontaneous decay rate from level $|i\rangle$ to level $|j\rangle$, γ_{ij} is the dephasing rate $\gamma_{ij} = (1/2)\sum_l \Gamma_{il} + (1/2)\sum_l \Gamma_{jl}$, and we have assumed a closed atomic system, i.e., $\rho_{11} + \rho_{22} + \rho_{33} + \rho_{44} = 1$.

In order to numerically prove the proposed tripod atomic system, we choose the cycling transition $F_e = 0 \leftrightarrow F_g = F_e + 1$ of a two-level atom subject to a DC magnetic field which induces a Zeeman splitting in two of the three lower levels. Such a transition can be implemented by considering the $4f^6 6s^2\,{}^7F_1 \leftrightarrow 4f^6 6s6p\,{}^5D_0$ in Samarium (Sm) (see Refs. [33,34]), among other atomic

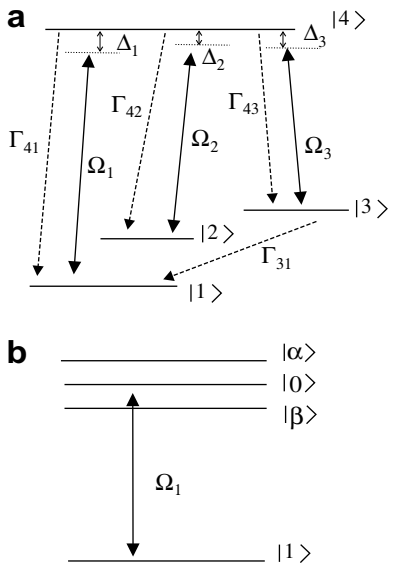

Fig. 1. (a) A tripod-type atom probed by field Ω_1 and driven by two control fields with Rabi frequencies Ω_2 and Ω_3. (b) Dressed states of the tripod-type atom. Transition between states $|1\rangle$ and $|0\rangle$ is only allowed while the control field Ω_3 is applied.

systems [35,36]. This scheme has also been addressed theoretically in the context of pump–probe configuration, showing the appearance of the so-called coherent hole burning at the Autler–Townes sidebands [37]. The existence of this atomic scheme will help us to show the feasibility of experimentally obtaining the results predicted in this work. Thus, we consider the case where transition $F_e = 0 \leftrightarrow F_g = 0$ ($|2\rangle \rightarrow |4\rangle$ in the notation used by us) is driven by a linearly polarized π field with Rabi frequency Ω_2, and transition $F_e = 0 \leftrightarrow F_g = 1$ ($|3\rangle \rightarrow |4\rangle$ in our notation) is driven by a circularly polarized σ_+ field, with Rabi frequency Ω_3. These two external fields will be used for optical engineering the atomic response. Finally, transition $F_e = 0 \leftrightarrow F_g = -1$ ($|1\rangle \rightarrow |4\rangle$ in our notation) is probed by a circularly polarized σ_- field Ω_1. In addition, in the numerical simulations we assume equal decay rates from the upper level, $\Gamma_{41} = \Gamma_{42} = \Gamma_{43} = \gamma$, and $\Gamma_{32} = \Gamma_{21} = 0$ and $\Gamma_{31} = 0.00175\gamma$ [34] which are adequate for the Sm atom.

3. Linear susceptibility of the system

Let us study the linear susceptibility of the tripod atomic system described above. Eq. (2) is the basis to analyze the probe absorption of a field probing $|1\rangle \rightarrow |4\rangle$. Thus, we set $\partial_t \rho_{ij} = 0$, and solve the resultant algebraic equations to obtain the steady-state values of populations and coherences. Fig. 2a shows the probe absorption $\mathrm{Im}(\rho_{41})$ versus the detuning Δ_1 for $\Omega_2 = \gamma$, $\Delta_2 = 0$, $\Delta_3 = \gamma$, and three different values of the control field Ω_3. In the case with $\Omega_3 = 0$, the atomic system behaves as a three-level Λ-type system, so we recover the standard EIT profile with a dark resonance at $\Delta_1 = \Delta_2 = 0$. However, when $\Omega_3 = \gamma$, a sharp absorption peak emerges, and simultaneously the point of transparency splits into two dark resonances, one located at $\Delta_1 = \Delta_2$ and the other at $\Delta_1 = \Delta_3$. This behavior was previously found by Paspalakis and Knight in a four-level atom in a tripod configuration [30]. The inspection of Fig. 2a reveals that the spectral position of the central absorption peak can be modified by changing the intensity of the control field Ω_3. We would like to remark that the ultranarrow peak has a subnatural linewidth, therefore a small change in the Rabi frequency of the control field leads the system from nearly transparency to high absorption. This striking behavior will be used latter in this work to produce switching of the $|1\rangle \rightarrow |4\rangle$ signal field by acting

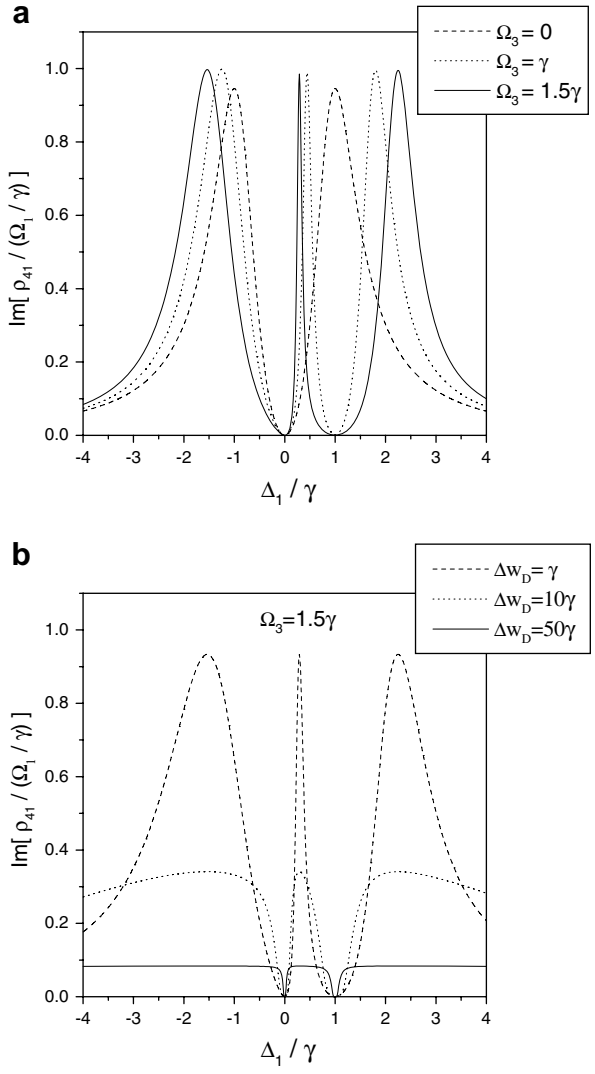

Fig. 2. (a) Normalized probe absorption of the $|1\rangle \rightarrow |4\rangle$ transition $\mathrm{Im}(\rho_{41})/(\Omega_1/\gamma)$ versus the probe detuning Δ_1 for several values of the Rabi frequency Ω_3. Other parameters are $\Delta_2 = 0$, $\Delta_3 = \gamma$, $\Omega_2 = \gamma$. $\Omega_3 = 0$ (dashed line) and $\Omega_3 = \gamma$ (dotted line) and $\Omega_3 = 1.5\gamma$ (solid line). (b) Doppler-broadened version of the normalized probe absorption $\mathrm{Im}(\rho_{41})/(\Omega_1/\gamma)$ versus the probe detuning for a control field $\Omega_3 = 1.5\gamma$, and several values of the Doppler width: $\Delta\omega_D = \gamma$ (dashed line), $\Delta\omega_D = 10\gamma$ (dotted line), and $\Delta\omega_D = 50\gamma$ (solid line).

on the $|3\rangle \rightarrow |4\rangle$ driving field. In addition, the peak value at the center of the above-mentioned absorption line takes similar values to those exhibited at the Autler–Townes doublet. The appearance of the central absorption line can be attributed to the coherence induced among the atomic levels by the interaction of the probe field Ω_1, and the control fields (Ω_2 and Ω_3) with the four-level system.

Let us consider the effect of Doppler broadening on the linear susceptibility of the tripod atomic system. In order to do that, we substitute the detunings Δ_j with $\Delta_j + \omega_{4j}v/c$, where v denotes the atomic velocity. Then, by using the probability distribution function we compute the average susceptibility of the probe laser

$$\rho_{41} = \int_{-\infty}^{\infty} \mathrm{d}v \frac{1}{v_\mathrm{p}\sqrt{\pi}} \mathrm{e}^{-v^2/v_\mathrm{p}^2} \rho_{41}(v), \tag{3}$$

where $v_\mathrm{p} = \sqrt{2kT/m}$ is the mean atomic velocity, and the Doppler width is given by $\Delta\omega_\mathrm{D} = 2\sqrt{\log 2}\omega_{41}v_\mathrm{p}/c$. The total probe absorption $\mathrm{Im}(\rho_{41})$ calculated through Eq. (3) is shown in Fig. 2b for different values of the Doppler width. For values of $\Delta\omega_\mathrm{D}$ below or close to the upper decay rate γ (see dashed line in Fig. 2b), the total probe absorption behaves as in the case without the Doppler broadening. Note that as the Doppler width increases above the decay rate value the probe absorption decreases although the positions of the EIT windows do not change. The high absorption central peak disappears for large values of $\Delta\omega_\mathrm{D}$ (see solid line in Fig. 2b). In the following and for the sake of simplicity, we neglect the Doppler broadening since the linear probe absorption does not change significantly for values of the Doppler width around the upper decay rate. In the case of larger values of $\Delta\omega_\mathrm{D}$, the main effect will be to reduce the sensitivity of the optical switching analyzed in this work, due to the reduction of the absorption curves.

In order to understand the behavior of the linear absorption of the tripod atomic system, we analyze the atomic system in the dressed state picture. To do that, the Hamiltonian corresponding to the atomic part and the external fields is diagonalized, i.e., we look for the λ_u and $|u\rangle$ that satisfy $H_\mathrm{P}|u\rangle = \lambda_u|u\rangle$ ($u = \alpha, \beta, 0$), where H_P is the part of the Hamiltonian in Eq. (1) which is related to the strong pump fields Ω_2 and Ω_3 and it is given by

$$\begin{aligned} H_\mathrm{P} = {} & \hbar\Delta_1\sigma_{44} + \hbar(\Delta_3 - \Delta_1)\sigma_{33} + \hbar(\Delta_2 - \Delta_1)\sigma_{22} \\ & - \hbar(\Omega_2\sigma_{42} + \Omega_3\sigma_{43} + \mathrm{H.c.}). \end{aligned} \tag{4}$$

The dressed states from Hamiltonian (4) to first order in Ω_3 are given by

$$\begin{aligned} |\alpha\rangle &\approx \frac{\Omega_R + \Delta_2/2}{D_\alpha}|4\rangle - \frac{\Omega_2}{D_\alpha}|2\rangle - \frac{\Omega_3(\Omega_R + \Delta_2/2)}{D_\alpha(\Delta_3 - \Delta_2/2 + \Omega_R)}|3\rangle, \\ |\beta\rangle &\approx \frac{\Omega_R - \Delta_2/2}{D_\beta}|4\rangle + \frac{\Omega_2}{D_\beta}|2\rangle + \frac{\Omega_3(\Omega_R - \Delta_3/2)}{D_\beta(\Delta_3 - \Delta_2/2 - \Omega_R)}|3\rangle, \\ |0\rangle &\approx \frac{\Omega_3|\Delta_2 - \Delta_3|}{D_0^2}|4\rangle - \frac{\Omega_2\Omega_3|\Delta_2 - \Delta_3|}{(\Delta_2 - \Delta_3)D_0^2}|2\rangle + \frac{|\Delta_2 - \Delta_3|}{(\Delta_2 - \Delta_3)}|3\rangle, \end{aligned} \tag{5}$$

where

$$\begin{aligned} D_\alpha &= \sqrt{(\Delta_2/2 + \Omega_R)^2 + \Omega_2^2}, \\ D_\beta &= \sqrt{(\Delta_2/2 - \Omega_R)^2 + \Omega_2^2}, \\ D_0^2 &= |\Delta_3(\Delta_2 - \Delta_3) + \Omega_2^2|, \end{aligned} \tag{6}$$

with $\Omega_R \equiv \sqrt{(\Delta_2/2)^2 + \Omega_2^2}$. The eigenvalues are $\lambda_\alpha \simeq \Delta_1 - \Delta_2/2 + \Omega_R$, $\lambda_\beta \simeq \Delta_1 - \Delta_2/2 - \Omega_R$, and $\lambda_0 \simeq \Delta_1 - \Delta_3$, respectively.

In the limit $\Omega_3 \rightarrow 0$, it can be clearly seen from Eq. (5) that dressed states $|\alpha\rangle$ and $|\beta\rangle$ correspond to the usual Autler–Townes components split by Ω_R, whereas the dressed state $|0\rangle$ corresponds to the bare state $|3\rangle$. However in the case with $\Omega_3 \neq 0$, and $\Delta_2 - \Delta_3 \neq 0$, the state $|0\rangle$ contains an admixture of level $|4\rangle$, thus it has a non-zero dipole matrix element with the ground state $|1\rangle$. Due to this coupling, transition from $|1\rangle$ to $|0\rangle$ becomes possible (see Fig. 1b). According to perturbation theory the transition probability from the ground state to the excited dressed states is given by

$$P_\mathrm{exc} \propto \left| \frac{\langle 1|\mu_{41}E_1|\alpha\rangle}{\lambda_\alpha} + \frac{\langle 1|\mu_{41}E_1|\beta\rangle}{\lambda_\beta} + \frac{\langle 1|\mu_{41}E_1|0\rangle}{\lambda_0} \right|^2. \tag{7}$$

The three terms within the angle brackets represent the three excitation paths corresponding to three-photon hyper-Raman resonances and interfere with each other. In order to justify the results shown in Fig. 2a, we set $\Delta_2 = 0$. Note that when $\Omega_3 = 0$, then $\langle 1|\mu_{41}E_1|0\rangle = 0$, and Eq. (7) reduces to the well-known expression for EIT in a Λ system. In this case the transition probability remains

$$P_\mathrm{exc} \propto \frac{1}{2}|\mu_{41}\Omega_1|^2 \left| \frac{1}{\Delta_1 + \Omega_2} + \frac{1}{\Delta_1 - \Omega_2} \right|^2, \tag{8}$$

which reduces to zero when $\Delta_1 = 0$, i.e., a dip appears at $\Delta_1 = 0$ due to destructive interference of the two possible paths $|1\rangle \rightarrow |\alpha\rangle$ and $|1\rangle \rightarrow |\beta\rangle$. On the other hand when $\Delta_2 = 0$, $\Omega_3 \neq 0$, and $\Delta_3 \neq 0$, the third term in Eq. (7) does not vanish, and the transition probability reads approximately as

$$P_\mathrm{exc} \simeq \frac{1}{2}|\mu_{41}\Omega_1|^2 \left| \frac{1}{\Delta_1 + \Omega_2} + \frac{1}{\Delta_1 - \Omega_2} + \frac{\sqrt{2}\Omega_3\Delta_3}{(\Delta_1 - \Delta_3)|\Omega_2^2 - \Delta_3^2|} \right|^2. \tag{9}$$

According to Eq. (9) a constructive interference occurs in the middle of the two resonances in agreement with the numerical results. The width of this peak depends on the strength of the additional control field Ω_3 as indicated by its presence in the numerator of Eq. (9).

In summary, the addition of an extra field to a conventional three-level Λ atom allows the modification of the position and width of the absorption peak and the double dark resonance by changing the intensity and detunings of the external fields.

4. Cavity field dynamics

In order to study the optical response of the atoms in a resonator, we consider a collection of such tripod atoms contained in a medium of length L and immersed in a unidirectional ring cavity (see Fig. 3). The incident coherent field E_I couples states $|1\rangle$ and $|4\rangle$ and propagates in the z direction. The cavity field $\mathscr{E}_1$ is given by

$$\mathscr{E}_1 = \frac{1}{2}E_1(z,t)e^{-i\omega_1 t} + \text{c.c.}, \tag{10}$$

$E_1(z,t)$ being the slowly-varying field envelope, $\Omega_1 \equiv \mu_{41}E_1/(2\hbar)$, where μ_{41} is the electric dipole moment of transition $|1\rangle \to |4\rangle$. The only field circulating in the ring cavity is the probe field E_1. Propagation of this laser field in the medium is governed by Maxwell's wave equation, which in the slowly varying envelope approximation reduces to

$$c\frac{\partial E_1(z,t)}{\partial z} + \frac{\partial E_1(z,t)}{\partial t} = i\frac{\omega_{41}}{\epsilon_0}P_1(\omega_1), \tag{11}$$

where $P_1(\omega_1) = N_a\mu_{41}\rho_{41}$ is the slowly oscillating term of the induced polarization oscillating at the angular frequency ω_1, with N_a the atomic density of the medium. The probe field E_I enters the cavity through mirror M_1, propagates in the cavity and interacts with the atomic sample of length L, then circulates in the cavity, and partially transmits out from the mirror M_2. The field boundary condition in the ring cavity is

$$E_1(t,0) = \sqrt{T}E_I + RE_1(t - t_0, L)e^{-i\theta}, \tag{12}$$

where R and T are the reflectance and the transmittance of the semi-silvered mirrors M_1 and M_2, respectively, t_0 is the cavity round-trip time, and θ is the phase due to the cavity detuning. Using the above condition we obtain the mean-field state equation

$$\frac{\partial\Omega_1}{\partial t} = -\kappa[(1 + i\phi_c)\Omega_1 - \Omega_I - i\gamma C\rho_{41}], \tag{13}$$

where $\kappa = cT/L$ is the cavity decay rate, $\Omega_I \equiv \mu_{41}E_I/(2\hbar\sqrt{T})$ is the Rabi frequency of the incident field, $\phi_c \equiv R\theta/T$, and C is the cooperation parameter defined as usual [1]

$$C = \frac{\omega_{41}\mu_{41}^2 N_a L}{2\hbar\epsilon_0 cT\gamma}. \tag{14}$$

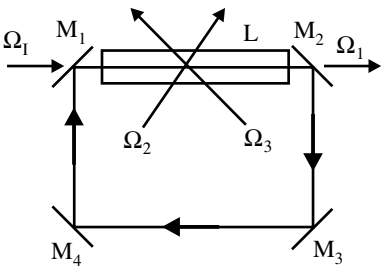

Fig. 3. Schematic diagram of a unidirectional ring cavity having four mirrors (M_1–M_4) and atomic sample of length L.

In the steady-state limit [1], we obtain the input–output relationship

$$|\Omega_I|^2 = |\Omega_1|^2\left\{\left[1 + C\,\text{Im}\left(\frac{\rho_{41}}{\Omega_1/\gamma}\right)\right]^2 + \left[\phi_c - C\,\text{Re}\left(\frac{\rho_{41}}{\Omega_1/\gamma}\right)\right]^2\right\}. \tag{15}$$

Eq. (15) resembles the well-known response of a two-level atom in a cavity. However, the main difference here is the possibility of controlling the susceptibility of the probe field, ρ_{41}, by acting on the detunings and/or Rabi frequencies of the other two optical fields. When only one driving field is present (say for example Ω_2), the system behaves as a Λ system. However, the addition of a second driving field Ω_3 produces the destruction of the exact two-photon resonance condition. This leads to large nonlinearities and simultaneously provides additional flexibility to manipulate the bistable response of the probe field by controlling the type of interference (constructive or destructive) or even most interestingly, inducing a double dark resonance.

We are now in position to compute the transmitted amplitude $|\Omega_1|$ of the probe beam under the influence of the control fields Ω_2 and Ω_3. A remarkable feature of the tripod-type atomic system is that optical memory and switching can be achieved without affecting the incident probe field.

4.1. Optical switching in the linear regime

We have shown in the previous section that the presence of both control fields leads to two holes in the linear absorption spectrum of the cavity field. A high absorption peak placed between the two holes emerges as a consequence of constructive interference. However, by turning off the control field Ω_3, the absorption peak disappears since the double dark resonance collapses into a single EIT window (see Fig. 2a). This interesting result could be used to switch the atomic response from high absorption to nearly transparency. In order to show this behavior, we consider a weak cavity field ($\Omega_1 \ll \gamma$), that is, a weak field is injected into the cavity ($\Omega_I = 0.1\gamma$). We use the same parameters as in Fig. 2a, that is, $\Omega_2 = \gamma$, $\Delta_2 = 0$, $\Delta_3 = \gamma$, and the cavity parameters $C = 100$, $\kappa = 0.1\gamma$, and $\phi_c = 0$. The driving field Ω_3 plays the role of the switching beam, changing its value from zero (switching beam off) to $\Omega_3 = \gamma$ (switching beam on) during the whole time evolution. For this purpose, we numerically solve the field equation (13) and the matter evolution equation (2). Fig. 4a shows the time evolution of the cavity field Ω_1 with detuning $\Delta_1 = 0.98\gamma$ when the control field Ω_3 is modulated as a train of rectangular pulses. When the control beam is off, a strong absorption peak occurs (see dashed line in Fig. 2a at $\Delta_1 \simeq \gamma$), then the amplitude of the output field is nearly zero. However, when the control beam is on, the system becomes transparent since a hole appears at that detuning value (see dotted line in Fig. 2a). Therefore, a high transmission of the cavity field takes place. In order to quantify

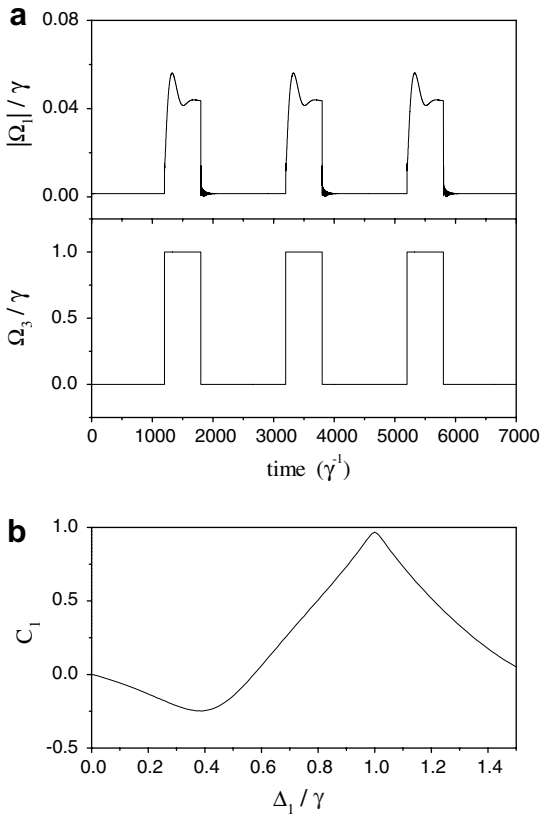

Fig. 4. (a) Time evolution of the cavity field Ω_1 when the control field Ω_3 is modulated as a train of "comb" pulses. The parameters are $\Omega_2 = \gamma$, $\Delta_1 = 0.98\gamma$, $\Delta_2 = 0$, $\Delta_3 = \gamma$, $C = 100$, $\phi_c = 0$, $\kappa = 0.1\gamma$, $\Omega_I = 0.1\gamma$. (b) Contrast of the cavity field defined in Eq. (16) versus the probe detuning Δ_1.

the effectiveness of this switch we define the contrast C_1 of the output signal as

$$C_1 \equiv \frac{|\Omega_1^{(\mathrm{on})}| - |\Omega_1^{(\mathrm{off})}|}{|\Omega_1^{(\mathrm{on})}| + |\Omega_1^{(\mathrm{off})}|}, \tag{16}$$

$\Omega_1^{(\mathrm{on})}/\Omega_1^{(\mathrm{off})}$ being the output cavity field when the control field is turned on/off. For the previous case considered in Fig. 4a, a very high contrast value is obtained ($C_1 \simeq 0.95$). Magnitude C_1 has been determined numerically as a function of the probe detuning Δ_1. The result is plotted in Fig. 4b. Two interesting regions appear at $\Delta_1 \simeq 0.4\gamma$ and $\Delta_1 \simeq \gamma$, where large contrast values are obtained. We can explain these results by looking at the linear absorption curves shown in Fig. 2a. In the case of $\Delta_1 \simeq \gamma$, the medium switches from high absorption to transparency when the control beam is turned on, as can be seen in Fig. 2a. At the other detuning value, $\Delta_1 \simeq 0.4\gamma$, the situation is the opposite: the medium switches from almost transparency to high absorption. This is the reason because of what the contrast value C_1 is negative at these detuning values. Note that in the vicinity of null detuning ($\Delta_1 \simeq 0$) and $\Delta_1 \simeq 0.56\gamma$, the contrast is almost zero since both absorption curves (Ω_3 on/off) take similar values.

Another interesting result found in the previous section is the possibility of controlling the position of the central high absorption peak by means of changing the amplitude of the driving field Ω_3. We will explore the use of this phenomenon to develop an ultra-sensitive all-optical switching. In this case we consider opposite detunings for both driving fields, i.e., $\Delta_2 = -\Delta_3$, since this configuration will allow us to obtain analytical results. The simultaneous interaction of both controlling beams leads to a linear absorption curve $\mathrm{Im}(\rho_{41})$ formed by three peaks and two transparency holes. A right (left) transparency hole at $\Delta_1 = \Delta_2$ ($\Delta_1 = \Delta_3$) should be expected which corresponds to the two-photon resonance condition of the cavity field with the controlling field Ω_2 (Ω_3). Therefore, the system can switch from high absorption to nearly transparency states by a very small change of one of the controlling fields. In order to illustrate the feasibility of this switching, we analyze the time evolution of the cavity beam Ω_1 at the center of the spectrum, $\Delta_1 = 0$. In the numerical simulation we consider a constant value of the controlling beam $\Omega_2 = 5\gamma$, whereas Ω_3 plays the role of the switching beam, changing its value between $\Omega_3^{(\mathrm{down})} = \Omega_2$ and $\Omega_3^{(\mathrm{up})} = \Omega_2 + \delta_\Omega$. The optical switching is shown in Fig. 5a, where the time evolution of the cavity field and the controlling beam are shown. We see in this figure that the output signal exhibits a significant change, from a very small value $|\Omega_1^{(\mathrm{down})}| \simeq 0.0018\gamma$ to a value equal to $|\Omega_1^{(\mathrm{up})}| \simeq 0.02\gamma$. In order to quantify the effectiveness of this optical switch we compare the contrast of the output signal

$$C_1 = \frac{|\Omega_1^{(\mathrm{up})}| - |\Omega_1^{(\mathrm{down})}|}{|\Omega_1^{(\mathrm{up})}| + |\Omega_1^{(\mathrm{down})}|}, \tag{17}$$

with the contrast of the switching field

$$C_3 = \frac{\Omega_3^{(\mathrm{up})} - \Omega_3^{(\mathrm{down})}}{\Omega_3^{(\mathrm{up})} + \Omega_3^{(\mathrm{down})}} = \frac{\delta_\Omega}{2\Omega_2 + \delta_\Omega}. \tag{18}$$

In the case shown in Fig. 5a, the contrast of the cavity field is close to $C_1 = 0.84$ whereas the corresponding to the switching field is $C_3 = 0.05$, thus revealing that a high ratio $C_1/C_3 \simeq 20$ can be obtained in this configuration. In order to maximize this contrast ratio we analyze C_1/C_3 as a function of the switching field step δ_Ω, i.e., Ω_3 is changing between Ω_2 and $\Omega_2 + \delta_\Omega$. The result is shown in solid line in Fig. 5b. This plot shows that there exists an optimum value of the switching field step which is close to $\delta_\Omega \simeq 0.1\gamma$. Since we are operating in the linear regime, we could perform an analytical study of the phenomenon. In the linear regime, the system of Eq. (2) may be linearized by assuming that, for a weak cavity field, ρ_{11} remains essentially constant and nearly equal to unity, thus $\rho_{22} \simeq \rho_{33} \simeq \rho_{44} \simeq 0$, while the only evolving quantities are coherences ρ_{41}, ρ_{21}, and ρ_{31}. Thus, keeping terms to first order in the probe cavity field Ω_1, and neglecting the inter-sublevel decay $\Gamma_{31} \simeq 0$, the steady-state solution of Eq. (2) is easily obtained, and the linear susceptibility of the probe transition is given by

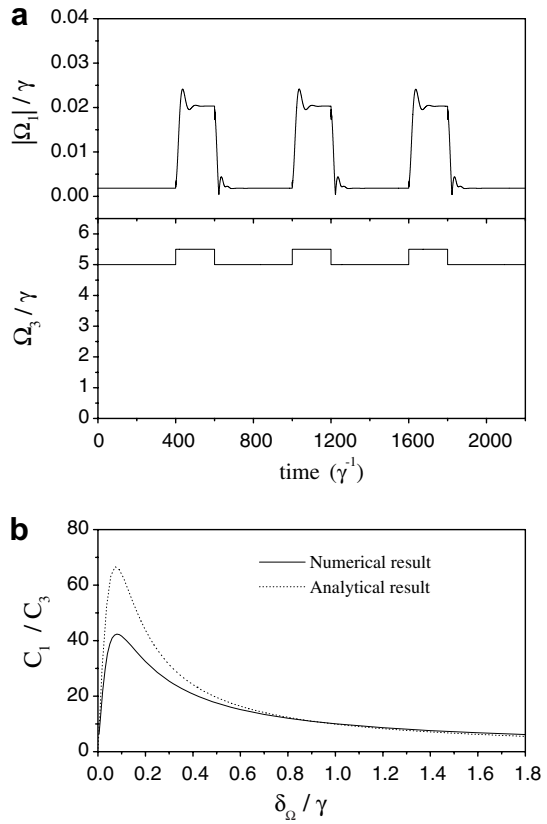

Fig. 5. (a) Time evolution of the cavity field Ω_1 and the control field Ω_3. The parameters are $\Omega_2 = 5\gamma$, $\delta_\Omega = 0.5\gamma$, $\Delta_1 = 0$, $\Delta_2 = 0.25\gamma$, $\Delta_3 = -0.25\gamma$, $C = 100$, $\phi_c = 0$, $\kappa = 0.1\gamma$, $\Omega_I = 0.1\gamma$. (b) Normalized contrast of the cavity field C_1/C_3 (defined in Eqs. (17) and (18)) versus the switching field step δ_Ω. Numerical result (solid line) and analytical result (dotted line).

$$\rho_{41} \simeq \frac{-\Omega_1(\Delta_1-\Delta_2)(\Delta_1-\Delta_3)}{(i3\gamma/2-\Delta_1)(\Delta_1-\Delta_2)(\Delta_1-\Delta_3)+(\Delta_1-\Delta_2)\Omega_3^2+(\Delta_1-\Delta_3)\Omega_2^2}. \tag{19}$$

The absorption curves obtained through Eq. (19) agree well with the linear absorption curves plotted in Fig. 2a. Furthermore, we compute from Eq. (19) the position of the central peak for the case $\Delta_2 = -\Delta_3$ (considering a small switching field step $\delta_\Omega < \gamma$)

$$\Delta_{1\text{peak}} = \frac{(\Omega_3^2-\Omega_2^2)\Delta_2}{\Delta_2^2+\Omega_2^2+\Omega_3^2} \simeq \frac{2\Omega_2\Delta_2\delta_\Omega}{\Delta_2^2+2\Omega_2^2}. \tag{20}$$

Eq. (20) reveals that the central peak shifts as the switching field step δ_Ω increases. Furthermore, Eq. (19) allows us to compute the full-width at half-maximum (FWHM) of the absorption peak, $\delta\Delta_1 \simeq 2\gamma\Delta_2^2/(\Delta_2^2+2\Omega_2^2)$. In order to switch the atomic response from high absorption at $\Delta_1 = 0$ to almost transparency, we should produce a displacement of the central peak in the absorption spectrum at least in the order of its FWHM. Therefore, the minimum switching field step δ_Ω which is required to displace significantly the absorption peak is given by $\delta_\Omega \simeq \gamma\Delta_2/\Omega_2$. This value is very close to the optimum value obtained through the numerical simulations (see solid line in Fig. 5b). Finally, we can use Eq. (19) to compute the ratio C_1/C_3. To do that, we set $\Delta_1 = 0$ and we take into account that $\delta_\Omega < \gamma$. After lengthy but straightforward calculations, we obtain

$$\frac{C_1}{C_3} \simeq \frac{2\Omega_2^3\delta_\Omega}{(\Omega_2\delta_\Omega)^2+(3\gamma/2)^2\Delta_2^2}. \tag{21}$$

Eq. (21) is plotted in Fig. 5b (dotted line) showing a good agreement with the numerical result. Using this simple expression, we can obtain the optimum value of the switching field step, being its value $\delta_\Omega^{(\text{opt})} = (3\gamma/2)\Delta_2/\Omega_2$ which gives a value close to 0.1γ, in agreement with the numerical result. The maximum achievable value for C_1/C_3 is $C_1/C_3 = \Omega_2^2/(3\Delta_2\gamma/2)$. The maximum value of C_1/C_3 obtained through the analytical curve (dotted line in Fig. 5b) is higher than the value given by the numerical one (solid line in Fig. 5b). The origin of this discrepancy relies on the fact that in the derivation of the analytical solution of ρ_{41}, the inter-sublevel decay Γ_{31} was neglected. The presence of this decay produces a non-zero spectral hole which reduces the transparency of the system and therefore gives a lower value of the contrast C_1 (see solid line in Fig. 5b).

In summary, the above results clearly demonstrate the controllability of the optical response by varying the amplitude and/or detuning of the driving field Ω_3.

4.2. Optical bistability and multistability

Now, we focus our attention to the case where the input field E_I is not in the linear regime. The nonlinear regime opens a rich scenario for engineering the atom-cavity dynamics. Note that Eq. (15) is a state equation which relates the transmitted amplitude $|\Omega_1|$ to the incident amplitude $|\Omega_I|$ and other parameters such as C, ϕ_c, Δ_i ($i = 1, 2, 3$), and the amplitudes of the control fields, Ω_2, and Ω_3. This equation incorporates contributions from absorption/dispersion which corresponds to the imaginary/real part of the effective susceptibility. This provides two different mechanism for bistability. In the current problem, it is rather difficult to have a closed form expression due to the high complexity of the dynamic equations. Therefore, we resort to obtain numerically the steady-state solution of density matrix equation (2) and the field equation (15).

Fig. 6a displays the bistable behavior of the four-level atomic system for several values of the control field Ω_3. We have used the parameter values employed in the calculations of the susceptibility in Fig. 2a ($\Omega_2 = \gamma$, $\Delta_2 = 0$ and

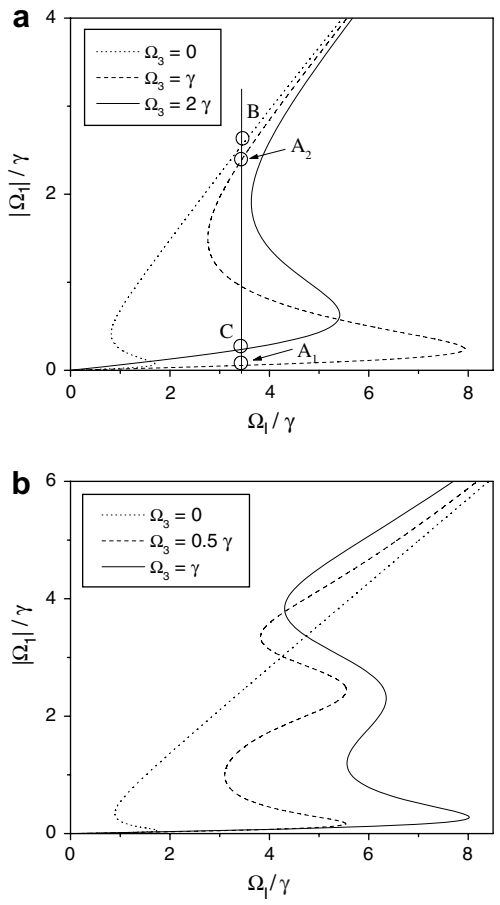

Fig. 6. Transmitted field $|\Omega_1|$ versus the incident one Ω_I. (a) *OB behavior*. The parameters are $\Omega_2 = \gamma$, $\Delta_1 = 0.5\gamma$, $\Delta_2 = 0$, $\Delta_3 = \gamma$, $C = 100$, $\phi_c = 1$. $\Omega_3 = 0$ (dotted line), $\Omega_3 = \gamma$ (dashed line), and $\Omega_3 = 2\gamma$ (solid line). The vertical line shows different steady-states (circle points) for the same input field. (b) *OM behavior*. The parameters are $\Omega_2 = 2\gamma$, $\Delta_1 = -1.5\gamma$, $\Delta_2 = \gamma$, $\Delta_3 = 0$, $C = 100$, $\phi_c = -1$. $\Omega_3 = 0$ (dotted line), $\Omega_3 = \gamma$ (dashed line), and $\Omega_3 = 2\gamma$ (solid line).

$\Delta_3 = \gamma$). We choose a probe detuning $\Delta_1 = 0.5\gamma$ which is in the middle of the two dark resonances where the narrow absorption peak occurs. In the case with $\Omega_3 = 0$, OB occurs for a very low threshold power (see dotted line in Fig. 6a). This behavior is not attributable to atomic optical saturation and it can be addressed by considering the dependence of the non-absorbing hole on the field intensity. This fact has been pointed out in previous works [15,25]. By solving Eqs. (2) and (13) with different initial conditions we have checked that the steady-state solutions displayed in Fig. 6a are stable in the regions of positive slope of the input–output curves. This the usual criterion in most of the cases of OB.

The four-level system opens new possibilities to manipulate quantum coherences in order to engineer the desired atomic response. Fig. 6a shows that the threshold and the width of the bistable region can be manipulated by changing the intensity of the control field Ω_3. In our case, it can be seen that OB appears for a great variety of space parameters, not only the one used to produce Fig. 6a.

The atomic polarization is a ratio of polynomials of high order on the field strength, so optical multistability (OM) can be reached for suitable parameters. This is illustrated in Fig. 6b where three curves corresponding to different values of the driving field ($\Omega_3 = 0$, $\Omega_3 = 0.5\gamma$, and $\Omega_3 = \gamma$) are plotted. It can be seen that the region of multistability can be controlled by the intensity value of this driving field.

4.3. Optical switching and storage in the bistable response regime

In the following, we are going to study the control of OB hysteresis curve by means of the control fields. Specifically, we will show that storage of optical signals can be achieved by appropriate shifts of the OB hysteresis curve. This behavior has been previously found in a four-level N-type atom by Chang et al. [27]. For this purpose we will use the OB curves analyzed in Fig. 6a. In the initial state the control field Ω_3 is considered to be "on" with an amplitude $\Omega_3 = \gamma$, therefore we start with the OB hysteresis curve shown in dashed line in Fig. 6a. If the control beam is turned off, the OB hysteresis curve shifts to the left part of the input–output graph (lower input fields), as it is shown in dotted line in Fig. 6a. On the other hand, if the control field is turned on with an amplitude $\Omega_3 = 2\gamma$, the hysteresis curve shifts to the right part of the input–output graph (higher incident fields), as is shown in solid line in Fig. 6a. This result means that we can control the transmission curve by means of the amplitude of the driving field Ω_3.

As an example, we consider a constant input cavity field $\Omega_I = 3.5\gamma$, a cavity decay rate $\kappa = 0.02\gamma$, and the control pulse sequence shown in Fig. 7. When the control beam is set to $\Omega_3 = \gamma$, the output field stays at the lower branch with a low power, in particular at state A_1 (see Figs. 6a and 7). Then, as the control beam Ω_3 is turned off, the system jumps to state B and when the control beam is set to its initial value $\Omega_3 = \gamma$, the system evolves into the upper branch at state A_2 (see Figs. 6a and 7). This last step leads to a small deep "written" on the transmitted pulse, thus, we

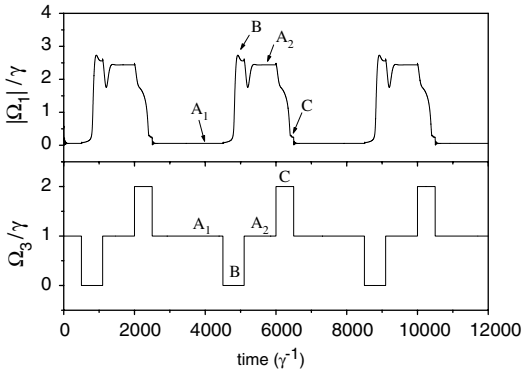

Fig. 7. Time evolution of the cavity field Ω_1 and the control field Ω_3. The parameters are $\Omega_2 = \gamma$, $\Delta_1 = 0.5\gamma$, $\Delta_2 = 0$, $\Delta_3 = \gamma$, $C = 100$, $\phi_c = 1$, $\kappa = 0.02\gamma$, $\Omega_I = 3.5\gamma$. The points indicated by the arrows are those corresponding to the encircled ones displayed in Fig. 6.

accomplish the storage of information. It is worth noting that we have got to trigger the system from the lower to the upper branch without changing the input field. The system will remain in this upper branch while the driving field does not change. To return to the lower branch we change the amplitude of the control beam to $\Omega_3 = 2\gamma$, so the system jumps to state C. When the control beam returns to the initial value $\Omega_3 = \gamma$, the system goes back to the lower branch at A_1. This controlling pulse sequence leads to optical switching and storage.

This switching process is different from the one considered in the previous section where the memory ability was not present.

5. Conclusions

We have investigated the atomic linear susceptibility of a probe field on a tripod-type four-level atom, under the influence of two control fields. It is found that the spectral position of the sharp absorption peak appearing between the two dark resonances can be modified by changing the intensity of one of the control fields. A remarkable feature is that this absorption line can be made subnatural so the sensitivity to lead the system from transparency to absorption can be made very strong. In fact, we have shown that the atomic response can switch from high absorption to nearly transparency, by turning on (off) or slightly varying one of the control fields. The system exhibits a high contrast ratio between the output signal and the auxiliary control field. The influence of the Doppler broadening on the previous results has been analyzed. Not significant changes have been found for values of Doppler width around the upper decay rate.

It is shown that by adding a second driving field to the usual three-level system, the exact two-photon resonance condition is destroyed, leading to an additional flexibility to control the type of interference (constructive or destructive). This originates that optical bistability and multistability can be obtained for a broad range of parameters, the threshold and width of the bistable region being controlled by changing slightly the intensity of one of the external fields, without affecting the input field. The controlled shift of the hysteresis curve allows us to obtain all-optical switching and storage of light signals.

Acknowledgments

This work has been supported by Projects No. FIS2004-03267 (MEC, Spain), PR45/05-14183 (UCM/CM, Spain), PR27/05-14019 (UCM/BSCH, Spain), and AE5/06-14369 (UCM, Spain).

References

[1] L.A. Lugiato, in: E. Wolf (Ed.), Progress in Optics, vol. 21, North-Holland, Amsterdam, 1984.
[2] S.E. Harris, J.E. Field, A. Imamoglu, Phys. Rev. Lett. 64 (1990) 1107.
[3] K.J. Boller, A. Imamouglu, S.E. Harris, Phys. Rev. Lett. 66 (1991) 2593.
[4] A. Kasapi, M. Jain, G.Y. Yin, S.E. Harris, Phys. Rev. Lett. 74 (1995) 2447.
[5] S. Shepherd, D.J. Fulton, M.H. Dunn, Phys. Rev. A 54 (1996) 5394.
[6] O. Kocharovskaya, Y.I. Khanin, JETP Lett. 48 (1988) 581.
[7] S.E. Harris, Phys. Rev. Lett. 62 (1989) 1033.
[8] M.O. Scully, S-Y. Zhu, A. Gavrielides, Phys. Rev. Lett. 62 (1989) 2813.
[9] G.G. Padmabandu, G.R. Welch, I.N. Shubin, E.S. Fry, D.E. Nikonov, M.D. Lukin, M.O. Scully, Phys. Rev. Lett. 76 (1996) 2053.
[10] S.E. Harris, J.E. Field, A. Kasapi, Phys. Rev. A 46 (1992) R29.
[11] M. Fleischhauer, C.H. Keitel, M.O. Scully, Ch. Su, B.T. Ulrich, S.-Y. Zhu, Phys. Rev. A 46 (1992) 1468.
[12] P. Zhou, S. Swain, Phys. Rev. A 56 (1997) 3011.
[13] G.S. Agarwal, Phys. Rev. A 18 (1978) 1490.
[14] D.F. Walls, P. Zoller, Opt. Commun. 34 (1980) 260.
[15] D.F. Walls, P. Zoller, M.L. Steÿn-Ross, IEEE J. Quantum Electron. QE-17 (1981) 380.
[16] W. Harshawardhan, G.S. Agarwal, Phys. Rev. A 53 (1996) 1812.
[17] H. Wang, D.J. Goorskey, W.H. Burkett, M. Xiao, Opt. Lett. 25 (2000) 1732.
[18] H. Wang, D.J. Goorskey, M. Xiao, Phys. Rev. A 65 (2002) 011801.
[19] A. Joshi, A. Brown, H. Wang, M. Xiao, Phys. Rev. A 67 (2003) 041801.
[20] A. Joshi, W. Yang, M. Xiao, Opt. Lett. 15 (2005) 905.
[21] D.A. Cardimona, M.G. Raymer, C.R. Stroud Jr., J. Phys. B: At. Mol. Phys. 15 (1982) 55.
[22] P. Zhou, S. Swain, Phys. Rev. Lett. 77 (1996) 3995.
[23] G.S. Agarwal, A.K. Patnaik, Phys. Rev. A 63 (2001) 043805.
[24] A. Joshi, W. Yang, M. Xiao, Phys. Lett. A 315 (2003) 203.
[25] M.A. Antón, O.G. Calderón, J. Opt. B: Quantum Semiclass. Opt. 4 (2002) 91.
[26] M.A. Antón, O.G. Calderón, F. Carreño, Phys. Lett. A 311 (2003) 297.
[27] H. Chang, H. Wu, C. Xie, H. Wang, Phys. Rev. Lett. 93 (2004) 213901.
[28] I. Novikova, A.S. Zibrov, D.F. Phillips, A. André, R.L. Walsworth, Phys. Rev. A 69 (2004) 061802.
[29] F. Vewinger, M. Heinz, R.G. Fernandez, N.V. Vitanov, K. Bergmann, Phys. Rev. Lett. 91 (2003) 213001.
[30] E. Paspalakis, P.L. Knight, J. Opt. B: Quantum Semiclass. Opt. 4 (2002) S372.
[31] D. Petrosyan, Y.P. Malakyan, Phys. Rev. A 70 (2004) 023822.
[32] S. Rebic, D. Vitali, C. Ottaviani, P. Tombesi, M. Artoni, F. Cataliotti, R. Corbalán, Phys. Rev. A 70 (2004) 032317.
[33] L.M. Barkov, D.A. Melik-Pashayev, M.S. Zolotorev, Opt. Commun. 70 (1989) 467.
[34] S.A. Diddams, J.C. Diels, B. Atherton, Phys. Rev. A 58 (1998) 2252.
[35] K. Bergman, H. Theuer, B.W. Shore, Rev. Mod. Phys. 70 (1998) 1003.
[36] P. Cerez, F. Hartmman, IEEE J. Quantum Electron. QE13 (1977) 344.
[37] Ying Gu, Qingqing Sun, Qihuang Gong, Phys. Rev. A 69 (2004) 063805.